Marine Pollution Bulletin 62 (2011) 140–153

Contents lists available at ScienceDirect

Marine Pollution Bulletin

journal homepage: www.elsevier.com/locate/marpolbul

Hindcast of oil-spill pollution during the Lebanon crisis in the Eastern Mediterranean, July–August 2006

Giovanni Coppini [a,b,*], Michela De Dominicis [a], George Zodiatis [c], Robin Lardner [c], Nadia Pinardi [b], Rosalia Santoleri [d], Simone Colella [d], Francesco Bignami [d], Daniel R. Hayes [c], Dmitry Soloviev [c], Georgios Georgiou [c], George Kallos [e]

[a] Istituto Nazionale di Geofisica e Vulcanologia, Sezione di Bologna, Italy
[b] Centro Interdipartimentale di Ricerca per le Scienze Ambientali, Università di Bologna, Ravenna, Italy
[c] Oceanography Centre, University of Cyprus, Nicosia, Cyprus
[d] Consiglio Nazionale delle Ricerche, Istituto per le Scienze dell'Atmosfera e del Clima, Rome, Italy
[e] University of Athens, Athens, Greece

ARTICLE INFO

Keywords:
Lebanese oil-pollution event
Oil-spill modeling
Operational oceanography
Remote sensing
Levantine Basin

ABSTRACT

MOON (Mediterranean Operational Oceanography Network http://www.moon-oceanforecasting.eu) provides near-real-time information on oil-spill detection (ocean color and SAR) and predictions [ocean forecasts (MFS and CYCOFOS) and oil-spill predictions (MEDSLIK)]. We employ this system to study the Lebanese oil-pollution crisis in summer 2006 and thus to assist regional and local decision makers in Europe, regionally and locally. The MEDSLIK oil-spill predictions obtained using CYCOFOS high-resolution ocean fields are compared with those obtained using lower-resolution MFS hydrodynamics, and both are validated against satellite observations. The predicted beached oil distributions along the Lebanese and Syrian coasts are compared with in situ observations.

The oil-spill predictions are able to simulate the northward movement of the oil spill, with the CYCOFOS predictions being in better agreement with satellite observations. Among the free MEDSLIK parameters tested in the sensitivity experiments, the drift factor appears to be the most relevant to improve the quality of the results.

1. Introduction

Accidental and illegal marine pollution in the Mediterranean Sea constitutes a major threat to the marine environment. Previous incidents in the Mediterranean Sea (e.g., Haven tanker, Ligurian Sea, 1991) and in European seas (e.g., Prestige tanker, Galicia, Spain, 2002) have resulted in environmental and economic damages (Loureiro et al., 2009) to fisheries, to the tourist industry and to coastal marine ecosystems. Oil-pollution discharges from ships in the Mediterranean have been described as significant (Pavlakis et al., 2001) and are a cause of environmental degradation in the Mediterranean Sea. To prevent the major impact of accidental oil spills, local and regional preparedness and response plans recommend the use of computer-aided support systems based on operational oceanography and real-time ocean forecasts coupled with satellite images and oil-spill models.

Operational Oceanography in the Mediterranean Sea was established in 2003 by the Mediterranean Operational Oceanography Network (MOON), which offers real-time services consisting of a set of Core Services (CS) and Downstream Services (DS). The CS deliver generic, all-purpose products based on observations and models, whereas the DS use CS products to formulate customized services for specific applications. One such DS service is the so-called decision-support system for oil-spill detection and forecasting, which will be described in this paper. This system consists of integrated satellite data and ocean-forecasting systems, MFS[1] and CYCOFOS[2], coupled with the MEDSLIK oil-spill model (Lardner and Zodiatis, 1998; Lardner et al., 2006). The satellite component integrates data received from recent-generation spectroradiometric and radar-satellite sensors, such as MODIS (on board AQUA since 2002 and TERRA since 2000) and ASAR (on board ENVISAT since 2002), making it possible to monitor the evolution of the oil pollution on a daily basis if needed. Remote sensing can provide substantial support to routine surveillance in open-ocean and coastal areas and has the advantage of being able to observe oil-spill events in remote and often inaccessible areas. Moreover, remote sensing can

* Corresponding author at: Istituto Nazionale di Geofisica e Vulcanologia, Sezione di Bologna, Italy.
E-mail address: coppini@bo.ingv.it (G. Coppini).

[1] http://gnoo.bo.ingv.it/mfs.
[2] http://www.oceanography.ucy.ac.cy/cycofos/forecast.html.

0025-326X/$ - see front matter © 2010 Elsevier Ltd. All rights reserved.
doi:10.1016/j.marpolbul.2010.08.021

provide information on the rate and direction of oil movement through multi-temporal imaging.

In this paper, we illustrate the application of the MOON oil-spill decision-support system to the largest oil-release accident in the Eastern Mediterranean, the Lebanese oil-pollution crisis, which occurred in mid-July 2006. The amount of oil released is considered the largest volume of oil ever dispersed in Eastern Mediterranean waters. MOON provided operational support, by means of MEDSLIK-CYCOFOS forecasts, to the operational response to the incident (Zodiatis et al., 2007, 2008b, 2008c).

This paper aims to demonstrate the strengths and weaknesses of the operational oil-spill monitoring and forecasting systems available today in the Mediterranean Sea.

CYCOFOS was run in real time; the MFS simulations have been carried out in delayed mode. In this paper, the MFS simulations will be compared with the CYCOFOS simulations and with satellite images from MODIS and ASAR. We also present the results of sensitivity experiments using different wind parameters and current depths.

The paper is organized as follows: Section 2 describes the remote-sensing systems used for oil-spill monitoring; Section 3 presents the forecasting model; Section 4 reports the hindcast experiments for the Lebanon crisis event, including sensitivity experiments; Section 4.2 presents the sensitivity experiments; and Section 5 summarizes our conclusions.

2. Remote sensing for oil-spill monitoring

Oil spills floating on the sea surface can be detected by Synthetic Aperture Radar (SAR) mounted on satellites (Fingas and Brown, 1997; Fiscella et al., 2000). Oil spills appear as darker areas due to the absence of short gravity and capillary waves, which normally backscatter the radar signal measured by SAR. Even though there are some limitations in the use of SAR data for oil-spill detection at very low (<3 m/s) and high wind speeds (>25 m/s), SAR has become a mature tool for oil-spill monitoring. The main limitations in the use of SAR are its long revisit time and the limited swath width of the sensors on board currently available satellite missions (ERS-2, ENVISAT and RADARSAT), which cannot guarantee seamless daily coverage. Table 1 gives an overview of the swath widths and revisit times of the SAR satellite instruments on board the abovementioned satellite platforms.

Remote-sensing devices for oil-spill detection include infrared video and photography, thermal-infrared imaging, and airborne laser fluorosensors. Airborne and space-borne optical sensors can complement SAR and contribute to cost-effective and reliable monitoring systems (Jha et al., 2008). Visible or optical sensors do not guarantee continuous all-weather coverage and usually suffer from reduced resolution capabilities compared to SAR; on the other hand, they allow monitoring of wider areas (at lower resolution).

Oil at the sea surface has a different reflectance than water in the visible region of the electromagnetic spectrum. The difference may be positive or negative, depending on the illumination-view angles (i.e., the solar and satellite azimuth and zenith angles of a given image pixel). Usually, positive differences (i.e., positive oil–water contrast) occur when an oil spill is in a high-glint region of the image (i.e., approximately mirror-like reflection conditions). Recent optical modeling (e.g., Otremba and Piskozub, 2001, 2004) has described the variability of such contrast with changes in illumination-view situations, film thickness and oil type. The main conclusion of these studies is that an oil film can generally be detected using VIS/IR sensors (see an application in Hu et al., 2003).

The medium resolutions of MODIS (250 m; http://modis.gsfc.nasa.gov) and MERIS (300 m; http://envisat.esa.int/instruments/meris/) channels show great potential for daily monitoring of oil spills because of their unprecedented synoptic and repetitive coverage (see also, Adamo et al., 2007; Shi et al., 2007; Lotliker et al., 2008).

In this paper, we show the potential capability of the synergetic use of active and passive sensors to monitor the Lebanon oil-spill incident. MODIS and ASAR imagery will be compared with model results to assess model-simulation performance.

Daily MODIS images from the AQUA and TERRA satellites were processed from 13 July to 27 August 2006, for a total of 72 scenes. ASAR satellite images were processed from 21 July to 27 August 2006, for a total of eight scenes. MODIS images were downloaded in the Level 0 format, which consists of raw data received from the satellite in standard binary form. After each image was processed to the Level 1B format for 36 spectral channels (http://oceancolor.gsfc.nasa.gov), seven spectral bands of the visible and near-infrared spectrum were extracted, and some were re-sampled at a spatial resolution of 250 m (two bands being already at 250-m resolution and the others at 500 m).

All seven bands were then graphically displayed as a color-coded reflectance image using IDL ENVI. Contrast stretching was performed to enhance local contrast in sections of the image containing oil slicks. Also, ENVI was used to compute band ratios (e.g., 645 and 859 nm L1B images) to further highlight oil slicks. The best band ratio was chosen by trial and error to maximize oil–water contrast based on the illumination-view conditions (glint or no-glint situation). Oil features were then manually digitized on these maximum-contrast images using the ENVI Region-Of-Interest (ROI) tool, and each oil-slick ROI was saved to a text file containing pixel latitude, longitude and reflectance in the various bands. This information was then used to extract oil-slick spectral properties, statistics for classification, masking, etc.

Processed ASAR images for use in this study were kindly provided by Telespazio SpA (http://www.telespazio.it). The Oceanography Centre of the University of Cyprus also processed MODIS data to verify the operational oil-slick predictions during the duration of the crisis. Analysis of the entire time series of ASAR and MODIS data for the Lebanon oil-pollution incident reveals that during the 43 monitored days, MODIS (with its daily coverage) provided useful information on the evolution of the oil spill for 24 days, whereas ASAR (because of its spatial and temporal coverage) contributed only 8 days of observations.

Table 1
Overview of the swath widths and revisit times of the SAR satellite instruments aboard the ERS-2, RADARSAT and ENVISAT satellite platforms and of the MODIS instrument aboard the TERRA and AQUA satellites.

Missions	Instruments	Type of measurement	Max swath width	Revisit time
ERS-2	SAR	Roughness	100 km	35 days
RADARSAT-2	SAR	Roughness	500 km	24 days[a]
ENVISAT	ASAR	Roughness	400 km	35 days[b]
ENVISAT	MERIS	Color	1150 km	3 days
TERRA and AQUA	MODIS	Color	2330 km	2 days

[a] http://www.radarsat2.info/about/mission.asp – selective looking can reduce the revisit time.
[b] http://envisat.esa.int/handbooks/asar/CNTR1-1-4.htm

It is therefore of great importance to integrate the information from these two sensors to perform monitoring at the space and time coverage required by the users.

3. The oil-spill forecasting systems

The oil-spill model used in this paper is MEDSLIK (Lardner and Zodiatis, 1998; Lardner et al., 2006). MEDSLIK consists of a drifting model with a representation of transformation processes to simulate the fate and dispersal of oil slicks. The spill is sub-divided into a large number (up to 100,000) of Lagrangian parcels of equal size.

The oil-parcel drift is given by two effects: deterministic advection by water currents and a turbulent-diffusive process. In finite-difference form, the position of each "*i*" oil parcel in space (x_i, y_i, z_i) and time is written as:

$$x_i(t+\tau) = x_i(t) + \{u(x_i,y_i,z_i,t) + \alpha(W_x(x_i,y_i,t)\cos\beta + W_y(x_i,y_i,t)\sin\beta)\}\tau + \Delta x_i^{(d)}$$

$$y_i(t+\tau) = y_i(t) + \{v(x_i,y_i,z_i,t) + \alpha(-W_x(x_i,y_i,t)\sin\beta + W_y(x_i,y_i,t)\cos\beta)\}\tau + \Delta y_i^{(d)}$$

$$z_i(t+\tau) = z_i(t) + \Delta z_i^{(d)} \quad (1)$$

where:

- $x(t+\tau), y(t+\tau), z(t+\tau)$ is the position of the parcel at time $(t+\tau)$;
- $u(x_i,y_i,z_i,t)$ and $v(x_i,y_i,z_i,t)$ are the zonal and meridional water-velocity components provided by the hydrodynamic model (MFS or CYCOFOS);
- W_x and W_y are the zonal and meridional components of the surface-wind vector;
- α and β are the so-called drift factor and drift angle;
- τ is the integration time step; and
- $\Delta x^{(d)}, \Delta y^{(d)}, \Delta z^{(d)}$ are the turbulent-diffusion terms written for a random-walk motion (Ahlstrom, 1975 and Hunter, 1987):

$$\Delta x_i^{(d)} = [2r-1]\sqrt{6k_h\tau}$$
$$\Delta y_i^{(d)} = [2r-1]\sqrt{6k_h\tau}$$
$$\Delta z_i^{(d)} = [2r-1]\sqrt{6k_v\tau} \quad (2)$$

where:

- K_h and K_v are horizontal and vertical diffusivities, chosen in our case to be constant and equal to $K_h = 2\ m^2/s$ and $K_v = 0.01\ m^2/s$; and
- r is a random value between 0 and 1.

The terms between parentheses in (1) are the deterministic components of the parcel movement; they consider the water-current velocities from the hydrodynamic model and a correction factor due to unresolved but deterministic processes. These terms are parameterized as a function of the wind-drift factor and the wind-drift angle. These correction factors have been interpreted in different ways in the literature of the past thirty years. Initially, this correction factor was chosen to account for unresolved Ekman currents at the surface because numerical models of water currents were coarse and inaccurate. The water-current values used in the eighties and before were mainly climatological and deduced from observations (i.e., they were approximately equal to the subsurface geostrophic currents). There was considerable dispute among modelers as to the best choices for the values of the drift factor and angle for Ekman currents; most models used a value of around 3% for the former and a value between 0° and 25° for the latter (Reed et al., 1994; Al-Rabeh, 1994).

With the advent of operational oceanography (Pinardi et al., 2003) and accurate operational models of circulation, Ekman processes have been resolved and are included in the water-current velocity (the terms with $u(x_i,y_i,z_i,t)$ and $v(x_i,y_i,z_i,t)$ in Eq. (1)).

In this paper, however, we will make the more traditional assumption for the wind drift and angle using the water-velocity field at a depth of 30 m. The choice of 30 m corresponds to the Ekman-layer e-folding depth, which for the Mediterranean Sea is generally between 10 and 30 m. Such an estimate is calculated using the scaling formula

$$\delta_E = \sqrt{\frac{K_v}{f}} \quad (3)$$

(Pond and Pickard, 1983), where f is the Coriolis parameter between 30 and 40 N and K_v is the vertical-eddy coefficient for momentum, which normally varies between 10^{-2} and $10^{-1}\ m^2\ s^{-1}$ near the surface. A depth of 30 m is therefore considered the average depth at which the effects of surface Ekman wind drift are significantly reduced. By using the water velocity at 30 m, the effects of Ekman-drift velocities can be safely added. If a current forecasting model is sufficiently fine to resolve the Ekman dynamics, the best choice should be to set the drift factor to zero and to use the water-surface flow from the Eulerian model.

The wind-correction factor can still be used to account for missing processes at the air-sea interface, such as wind-wave-induced currents. The Stokes drift is in fact proportional to the wind speed (i.e., wind-drift angle equal to zero) (Rascle et al., 2006, 2008; Ardhuin et al., 2009). Several other deterministic corrections could be considered, but in this paper we use only the traditional wind-drift factor (3%) with water currents at 30 m, a wind-drift angle equal to 0.0 (Reed et al., 1994; Al-Rabeh, 1994) and an overall wind-drift factor of 1.2% with zero angle related to wave effects on the surface currents (Rascle et al., 2006, 2008; Ardhuin et al., 2009).

MEDSLIK includes fate processes, such as evaporation of the lighter oil fractions, mixing into the water column by wave action, emulsification and beaching on the coast (Mackay and Paterson, 1980; Mackay and Leinonen, 1977). Changes in the viscosity and density of the oil are computed according to the amount of emulsification and evaporation of the oil itself. Input data for the model are the date and time of the start of the spill, duration of the spill, location of the spill, type of oil and volume of the spill. The output is given in terms of trajectories of oil parcels and their corresponding oil properties (i.e., evaporated and emulsified oil percentages and presence on the surface or dispersed in the water column).

The buoyant effect is not taken into account in the vertical process of Eq. (1). This is the approach used in MEDSLIK: the particles are mass-less and no gravity velocity is calculated or used. The only process that is taken into account for the vertical movement of the oil particles is the vertical turbulent diffusion. This diffusion is applied to a certain number of particles that is defined by the weathering processes. At the beginning of the simulation, all the particles are released at the sea surface. As part of the weathering process, a volume of particles that have dispersed in the water column is calculated. The volume of dispersed particles is transformed into a probability of dispersion (P), which is subsequently used to determine which particles will be dispersed. For each particle that is defined as dispersed, a new depth (z_i) is calculated as result of the turbulent diffusion in the vertical direction of Eqs. (1) and (2). The particle will therefore be advected by the horizontal-currents field at depth (z_i).

MFS (Pinardi et al., 2003) produces daily mean analyses (from a combination of modeling and observations) on a weekly basis and daily mean or hourly mean 10-day forecasts on a daily basis. The system consists of a numerical model (Tonani et al., 2008) and a data-assimilation scheme (3DVAR) (Dobricic and Pinardi, 2008)

capable of assimilating all the available satellite and in situ data. The horizontal resolution of MFS is 1/16 * 1/16 degrees, approximately 6 km, and 72 unevenly spaced vertical levels (Tonani et al., 2008). The model is run with a time step of 600 s. MFS is forced by atmospheric forcing produced by the European Center for Medium range Weather Forecast-ECMWF analyses and forecasts (ECMWF, 2005) at 0.5 * 0.5 degrees and 6-hour resolution. The water flux is computed from a monthly mean climatology for precipitation ("CMAP", Climate Prediction Center CPC, Merged Analysis of Precipitation[3]) and a monthly climatology for river runoff, and evaporation is computed from the atmospheric forcing (ECMWF) at 6-hour resolution. The MFS analyses and forecasts are compared once a week with observations, providing quality control and assessment of the products. This continuous evaluation of the system's performance and data assimilation make the operational oceanography of the last ten years a major step forward compared to the modeling systems of past decades.

The MFS products are used by the nested ALERMO sub-regional forecasting system (Sofianos et al., 2006), and the ALERMO output is then used as boundary and initial conditions for the nested CYCOFOS high-resolution forecasting system. The CYCOFOS high-resolution model (Zodiatis et al., 2003, 2008a) is forced by atmospheric forcing produced by the SKIRON high-frequency forecasting systems at 5 km * 5 km and 1-hour resolution. CYCOFOS covers an area of the NE Levantine Basin in the Eastern Mediterranean (31°00′E–36°13′E and 33°00′N–36°55′N). The horizontal resolution of CYCOFOS is 1.8 km (1 nm) with 284 × 206 horizontal grid points. The CYCOFOS model has a time step of 240 s. In the vertical dimension, a non-uniform grid of 25 sigma layers is used with exponentially decreasing spacing near the surface and sea bed to provide finer resolution of the surface and sea-bed layers (Zodiatis et al., 2008a). CYCOFOS produces 6-hourly mean forecasts for the next four-and-a-half days on a daily basis. The CYCOFOS ocean forecasts have received extensive validation and inter-comparison with the parent models and with remote and in situ observations (Zodiatis et al., 2008a).

Notably, tidal forcings and other high-frequency forcings that are not explicitly resolved by the operational models used (MFS and CYCOFOS) could play a relevant role in oil transport and transformation processes. However, one of the main goals of this work is to evaluate the performance of the two operational forecasting systems (MFS and CYCOFOS) in oil-spill forecasting.

4. Hindcast experiments of the Lebanon oil-pollution event

The spill occurred in mid-July 2006 from the Jieh power plant, which is located 30 km south of Beirut (Fig. 1 a and b) is now believed that the spill occurred as a result of two bombing raids on the mornings of 13 and 15 July. Different press releases reported the bombing of the power plant on the 13 and 15 July. The available MODIS image shows smoke plumes from the Jieh Power plant on 16 July 2006 at 8:30 GMT (Fig. 2), whereas no smoke is visible in the MODIS image dated 15 July at 11:00 GMT (not shown). Therefore, it is possible that the bombing event occurred on 13 July but the power plant started to burn only on 16 July. This lack of information causes uncertainties about the starting date of the spill and the duration of the spill. The amount of oil spilled was variously reported as being between 15,000 and 20,000 tons. According to UNEP information (UNEP, 2007), the oil contained in the tanks was heavy IFP–number 6 fuel[4], which has the following key properties:

- High viscosity or resistance to flow, resulting in low mobility of the oil.
- High density (950–1030 kg/m^3).
- Tendency to break up into tar balls and sink to the bottom when released into water.
- Low volatility, leading to low fuel evaporation.

The spill was modeled as a continuous leakage of oil over a period of 144 h or 6 days starting from 13 July 2006, with a total mass of 18,770 tons of oil released during this time.

The hindcast experiments were carried out using MEDSLIK coupled with CYCOFOS and MFS. The water-current fields for 16 July 2006 from CYCOFOS (Fig. 3) showed a northerly flow parallel to the coasts of Lebanon and Syria, with flow velocities in the 20–30-cm/s range. This flow eventually turned westward to form the Asia Minor current in the Cilician Basin. This flow regime was similar to the climatological flow regime known for this region (Pinardi et al., 2006). The departure from a northerly flowing current along the Lebanese and Syrian coasts has also been registered previously but in a more episodic manner (Brenner, 2003).

These features persisted for the next 2 months, apart from the occasional development of small eddies in the lee of the various headlands. In the gulf of Beirut, a detachment of the currents from the coasts and the formation of a stagnation-like circulation were noted. This pattern might be interpreted as an anticyclonic eddy localized in the Gulf. However, the model resolution does not allow the complete reconstruction of this flow field. Sea-surface temperature in the same period from CYCOFOS (Fig. 4) and along the affected coastal areas was as high as 30 °C. The high-frequency SKIRON wind forecast (Fig. 5) showed winds varying in direction from south-westerly to north-westerly. This wind pattern remained steady for most of the months of July and August 2006, with wind strength varying generally between 2 and 7 m/s.

During the first day of the spill, the northward currents were present (Fig. 3), whereas the flow field of 14 July 2006 in front of the power plant appeared weaker and unstable (not shown). In the following days, the northward current flow in front and north of the Jieh power plant became steady, and the anticyclonic eddy in the gulf of Beirut appeared to be stable. The northward current returned closer to the coast north of the Gulf of Beirut and strengthened, whereas in front of the Jieh power plant the currents weakened during 21–23 July 2006 (Fig. 6). The flow intensity along the coast north of Beirut appeared to decrease around 27 July 2006 and then to increase again during the end of July. The northward direction of the flow along the coast and the intensity of the currents appeared steady in the first half of August 2006.

4.1. Reference experiments

The hindcast experiments of this study are reported in Table 2. The experiments were designed to test the impact of water currents from MFS and CYCOFOS, the wind-factor and angle parameters and the depth of the water currents considered. In experiments 1 and 2, water currents were taken at a depth of 30 m and the wind parameter was fixed at 3%. In experiments 3 and 4, water currents were taken at the surface and the wind parameter was fixed at 0%. In experiments 5 and 6, water currents were taken at the surface and the wind parameter was fixed at 1.2%.

Experiment 1 was also run in real time during the actual oil-spill accident. Comparisons of oil-slick position and extent detected by satellite images (MODIS and ASAR) and simulated oil at sea from experiment 1 (using CYCOFOS) and experiment 6 (using MFS) are presented in Figs. 7–11. Oil-slick regions digitized from MODIS images are shown in green so as to be more easily compared with the model simulations.

[3] Monthly CMAP estimates back to the 1979 are available from CPC ftp server (ftp://ftp.cpc.ncep.noaa.gov/precip/cmap).

[4] Information on n.6 fuel oil at http://en.wikipedia.org/wiki/Fuel_oil.

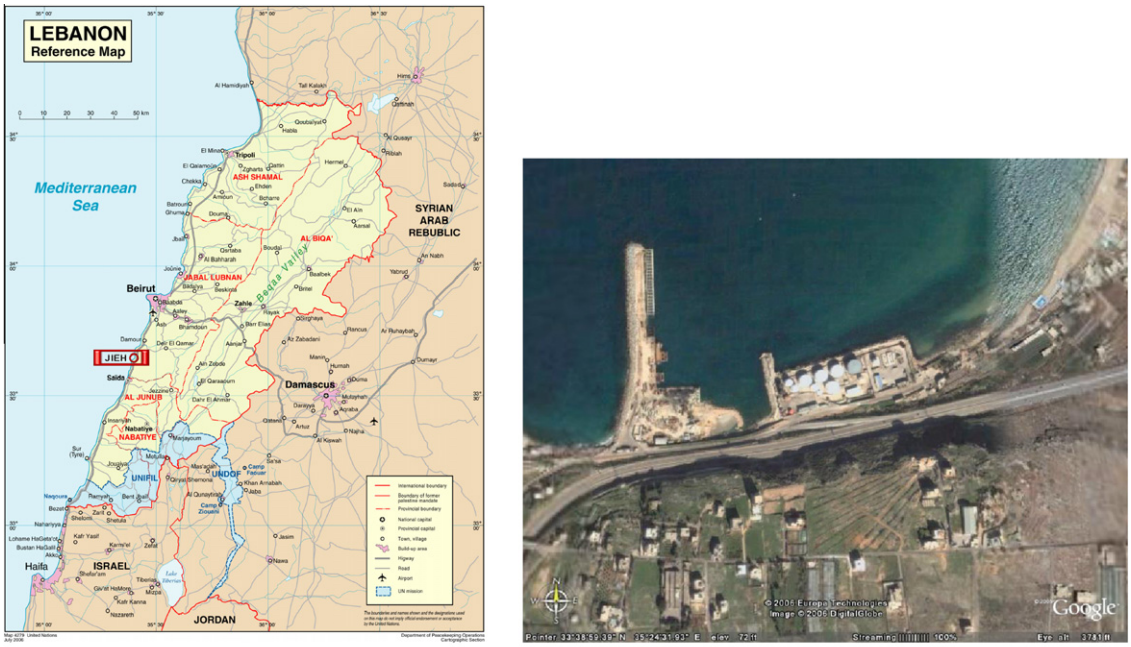

Fig. 1. (a) Geographical position of Jieh; (b) on-shore position of the Jieh power station taken from Google Earth before the crisis.

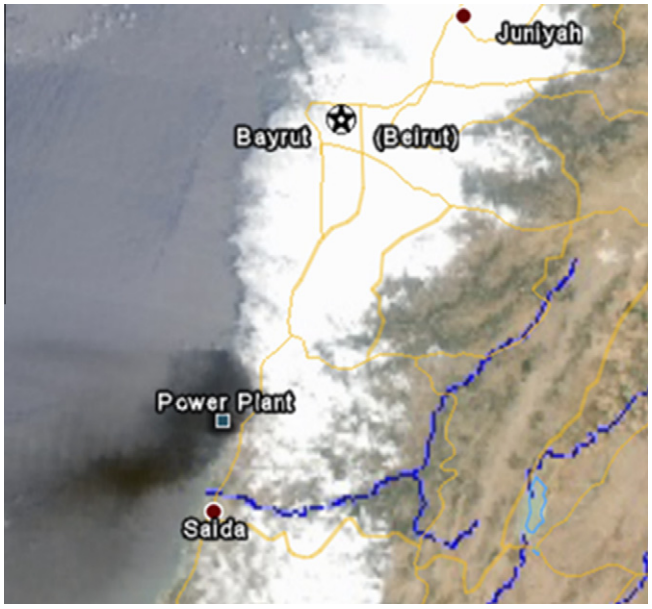

Fig. 2. MODIS AQUA image from 16 July (08:30 GMT). A black smoke plume is visible and bombing has occurred.

Fig. 3. Surface-currents field for 16 July 2006 at 12:00 from the CYCOFOS forecasting system. Dark arrows represent current directions and intensity in cm/s.

The first comparison between satellite images and model outputs is given in Fig. 7 for 19 July, when the MODIS AQUA image (2006 10:35, 19 July) shows that the smoke plume (blue) was still rising from the power plant and the oil (yellow–brown) had reached the Gulf of Beirut and Byblos. Both the CYCOFOS (Fig. 7b) and MFS (Fig. 7c) simulations showed that the spilled oil was transported northward: CYCOFOS forecasted the oil offshore in the Gulf of Beirut, similar to the pattern of the oil spill as seen in the satellite image. The MFS simulation showed the oil offshore in the Gulf of Beirut and off Byblos, in agreement with the satellite observations but perhaps too far offshore.

On 21 July, an ASAR image (Fig. 8a) was available showing the oil in the Gulf of Beirut reaching Byblos. The CYCOFOS predictions (Fig. 8b) showed progressive transport of the oil northward, closely reproducing the pattern of the oil in the Gulf of Beirut and north of Tripoli. MFS predictions (Fig. 8c) also showed northward displacement of the slick but seemed to overestimate the oil in the Gulf of Beirut and continued to show an unrealistic offshore extent of the slick due to the offshore starting position and the coarse model resolution.

On 23 July, the satellite image (Fig. 9a) showed the oil spill in the Gulf of Tripoli to be closely simulated by the CYCOFOS hindcast (Fig. 9b); however, the hindcast seemed to underestimate the

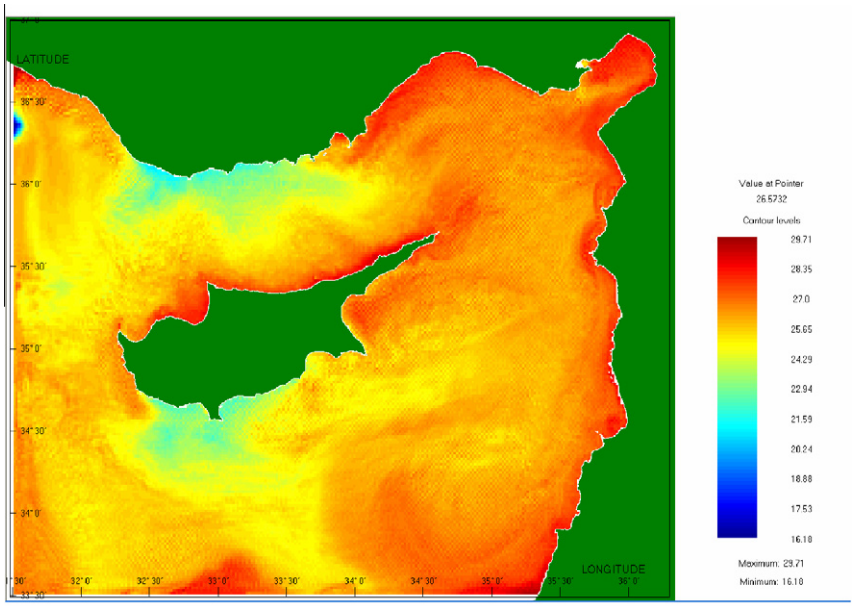

Fig. 4. CYCOFOS surface-temperature fields for 15 July 2006.

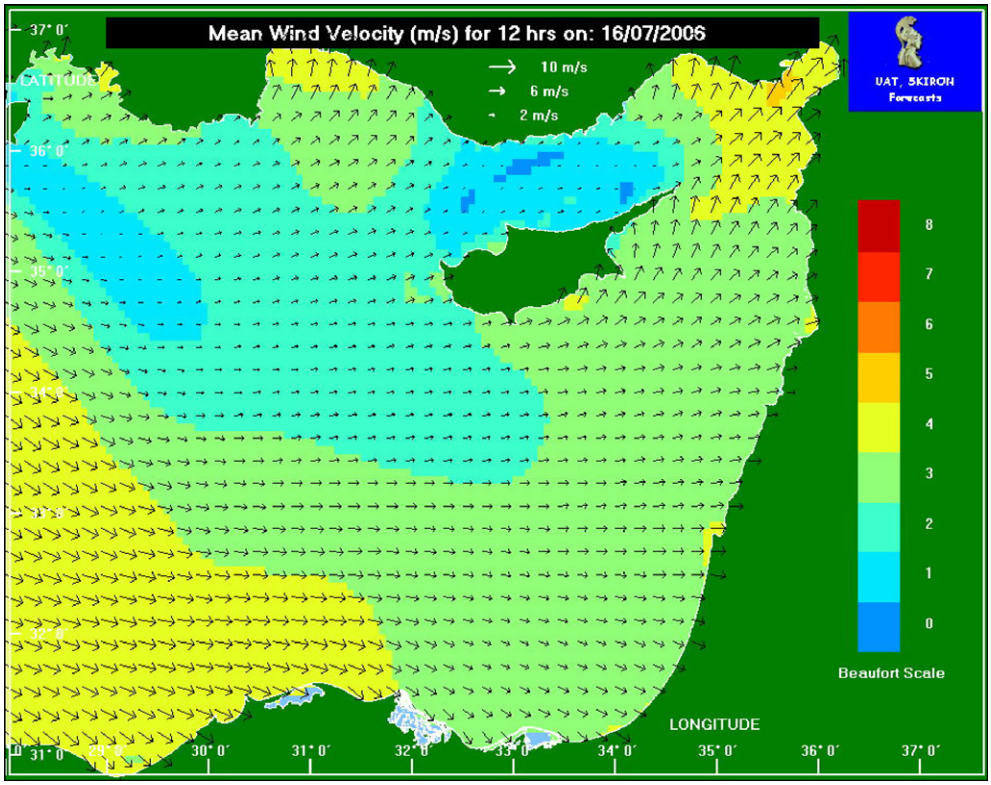

Fig. 5. Mean wind-velocity field for 16 July 2006 at 12:00 from the SKIRON forecasting system. Dark arrows represent wind directions and intensity in m/s. Wind intensity is also shown by the color scale in the background.

offshore extent of the oil slick and overestimate the northward extent of the slick. However, the northernmost part of the coast was not covered by satellite images due to clouds. The offshore part of the slick was closely reproduced by MFS, except in the southern portion (Fig. 9c), and the MFS predictions seemed to underestimate the northernmost extent of the slick.

The oil continued to move northward; on 2 August (Fig. 10a), the oil spill reached Tartus. The CYCOFOS prediction (Fig. 10b) showed good agreement with the satellite image, but the model still underestimated the offshore extent of the slick in the Gulf of Tartus and in the Gulf of Beirut. The MFS prediction (Fig. 10c) agreed well with the satellite observations in the Gulf of Tartus, but the model underestimated the oil in the Gulf of Beirut and overestimated the northernmost extent of the observed slick.

An ASAR image was also available for 6 August (7:51 GMT); Fig. 11 presents both the MODIS TERRA 8:50 GMT image

Fig. 6. Surface-currents field for 23 July 2006 at 12:00 from the CYCOFOS forecasting system. Dark arrows represent current directions and intensity in cm/s.

Table 2
Summary of model runs and sensitivity experiments. In experiments 1 and 2, the hydrodynamics models MFS and CYCOFOS and the oil-spill model MEDSLIK were used in the basic configuration. Experiments 3, 4, 5 and 6 evaluated the responses of MFS to changes in the wind parameters and in the current-transfer depth.

	Experiment 1	Experiment 2	Experiment 3	Experiment 4	Experiment 5	Experiment 6
Current field	CYCOFOS (6-hourly forecast)	MFS (1-hourly mean forecast)	CYCOFOS (6-hourly forecast)	MFS (1-hourly mean forecast)	CYCOFOS (6-hourly forecast)	MFS (1-hourly mean forecast)
Wind field	SKIRON (1-hourly forecast)	ECMWF (6-hourly mean forecast)	SKIRON (1-hourly forecast)	ECMWF (6-hourly mean forecast)	SKIRON (1-hourly forecast)	ECMWF (6-hourly mean forecast)
Spill position	33°40′N 35°24.75′E	33°41′N 35°10′E	33°40′N 35°24.75′E	33°41′N 35°10′E	33°40′N 35°24.75′E	33°41′N 35°10′E
Start spill date	13/07/2006 08:00	13/07/2006 08:00	13/07/2006 08:00	13/07/2006 08:00	13/07/2006 08:00	13/07/2006 08:00
Spill duration	144 h	144 h	144 h	144 h	144 h	144 h
Total mass of spill	18,770 tons	18,770 tons	18,770 tons	18,770 tons	18,770 tons	18,770 tons
Type of oil	API = 20	API = 20	API = 20	API = 20	API = 20	API = 20
Wind-correction factor	3%	3%	0	0	1.2%	1.2%
Wind angle factor	0	0	0	0	0	0
Current depth	30 m	30 m	Surface	Surface	Surface	Surface
Number of particle released	90,000	90,000	90,000	90,000	90,000	90,000

(Fig. 11a) and the ASAR image at 7:51 GMT (Fig. 11b). The MODIS-ASAR comparison highlights that the method used to detect the oil spill in the visible bands of MODIS works well. In fact, the slick patch (green) localized in the Beirut area matches the pattern retrieved in the ASAR image. In the portion of the sea close to Tartus, however, clouds preclude the detection of the oil slick by the visible sensor, whereas slicks are present in the ASAR picture. Nevertheless, it is possible to detect the presence of a slick in a partially cloud-free area south of Latakia in the MODIS picture. The importance of integrating information from the two satellite datasets is obvious: under clear-sky conditions, MODIS can monitor an area of interest twice a day, resolving the temporal evolution of the event, whereas ASAR validates the MODIS image and provides information in cloudy areas. The CYCOFOS prediction seems to reproduce well the evolution of the oil slick apart from underestimation of the northernmost extent of the slick. The MFS prediction seems to underestimate the oil in the Gulf of Beirut but closely reproduces the oil detected south of Tartus in the ASAR image. MFS overestimates the northernmost component of the slick.

Oil on the Lebanese coastline was observed and reported first by the Lebanese Ministry of Environment, by the Green Line Association (GLA, 2007), by the Experts Working Group for Lebanon in

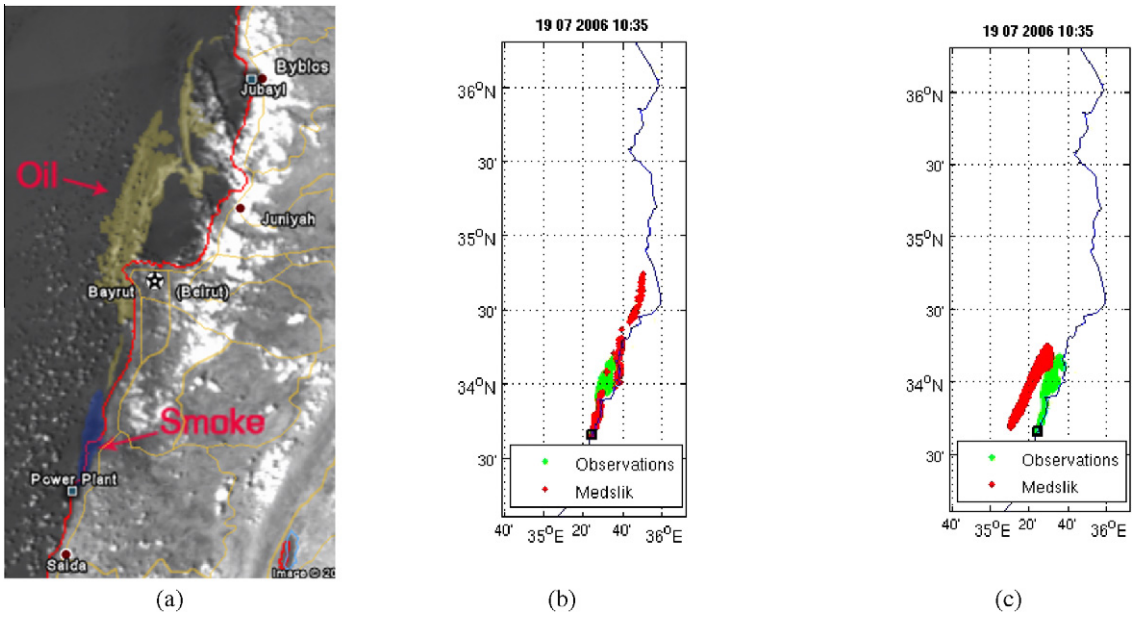

Fig. 7. Panel (a) shows the MODIS AQUA image from 19 July 2006 at 10:35 GMT. Panel (b) shows the position of the oil slick on 19 July at 11:00 GMT (after 147 h) as predicted by CYCOFOS. Panel (c) shows the position of the oil slick on 19 July 2006 at 11:00 GMT (after 147 h) as predicted by MFS. (a) July 19 (10:35 GMT): enhanced image. Smoke plume (blue) is still rising from the power plant. Oil (old, yellow) has reached the gulf of Beirut and Byblos. (b) The position of the oil slicks (red) on 19 July at 11:00 GMT (after 147 h) as predicted by CYCOFOS. (c) The position of the oil slicks (red) on 19 July at 11:00 GMT (after 147 h) as predicted by MFS.

2006 (EWGL, 2006) and by a World Bank report (World Bank, 2007). In particular, the Lebanese Ministry of Environment informed the CYCOFOS team on 4 August 2006 that the operational MEDSLIK oil-spill predictions on the beached oil were in agreement with their observations. Fig. 12 presents the areas of the Lebanese coast that have been reported to be impacted by oil pollution. Observations of oil on the Syrian coast are few; according to the declarations of Syrian Government representatives, a first 'wave' of oil arrived on the coast on 26 July and a second 'wave' arrived on 2 August (IMO/REMPEC and Joint UNEP/OCHA, 2006). According to the Expert mission in Syria (REMPEC, 2006 and Amato and Alcaro, 2006), oil residues affected beaches along the coast of Syria from the Lebanese border to Baniyas, 50 km north of Tartus. After cleaning operations had occurred, oil residues were collected at the following locations in Syria by a delegation of international experts (IMO/REMPEC, 2006): at the Lebanese/Syrian

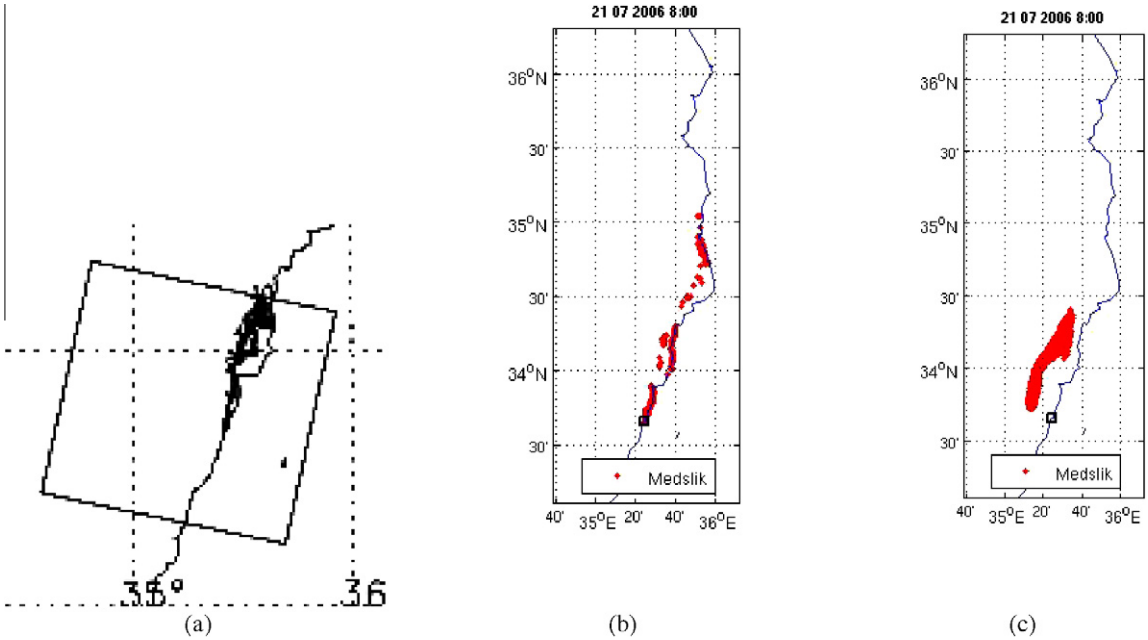

Fig. 8. Panel (a) shows the ASAR ENVISAT image for day 21. The ASAR image is compared with the position of the oil slick as predicted by CYCOFOS (panel b) and by MFS (panel c). (a) July 21 (07:49): ASAR Envisat image. Oil spill (black) is mostly located in the gulf of Beirut but has already reached Chekka, located south of Tripoli. (b) The position of the oil slicks (red) as predicted for 21 July at 8:00 GMT (after 192 h) by CYCOFOS. (c) The position of the oil slicks (red) predicted for 21 July at 8:00 GMT (after 192 h) by MFS.

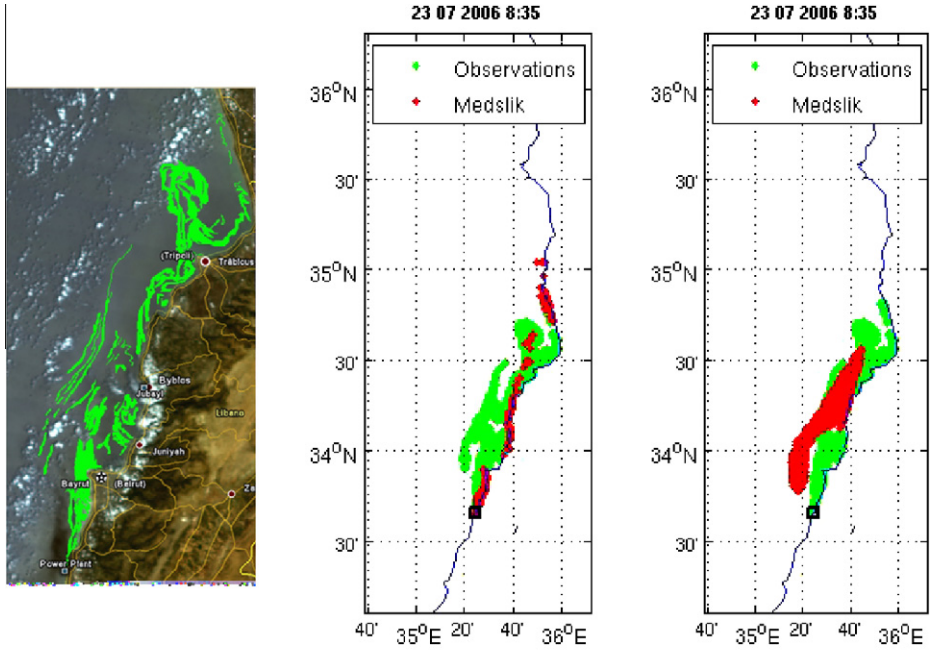

Fig. 9. Panel (a) shows the MODIS AQUA images from 23 July 2006, 8:35 GMT. The observed positions of the oil slicks (panel a) are compared with the positions predicted by CYCOFOS (panel b) and by MFS (panel c). (a) Magnified portion of the MODIS-ACQUA image from 23 July at 08:35 GMT: oil (green) is already in Tripoli. Mushroom-like feature. (b) The positions of the oil slicks and oil concentrations predicted by CYCOFOS (red) on 23 July at 9:00 GMT (after 241 h) compared with the slick observed by MODIS (green), also shown in image 9 (a). (c) The positions of the oil slicks and oil concentrations predicted by MFS (red) on 23 July at 9:00 GMT (after 241 h) compared with the slick observed by MODIS (green), also shown in image 9 (a).

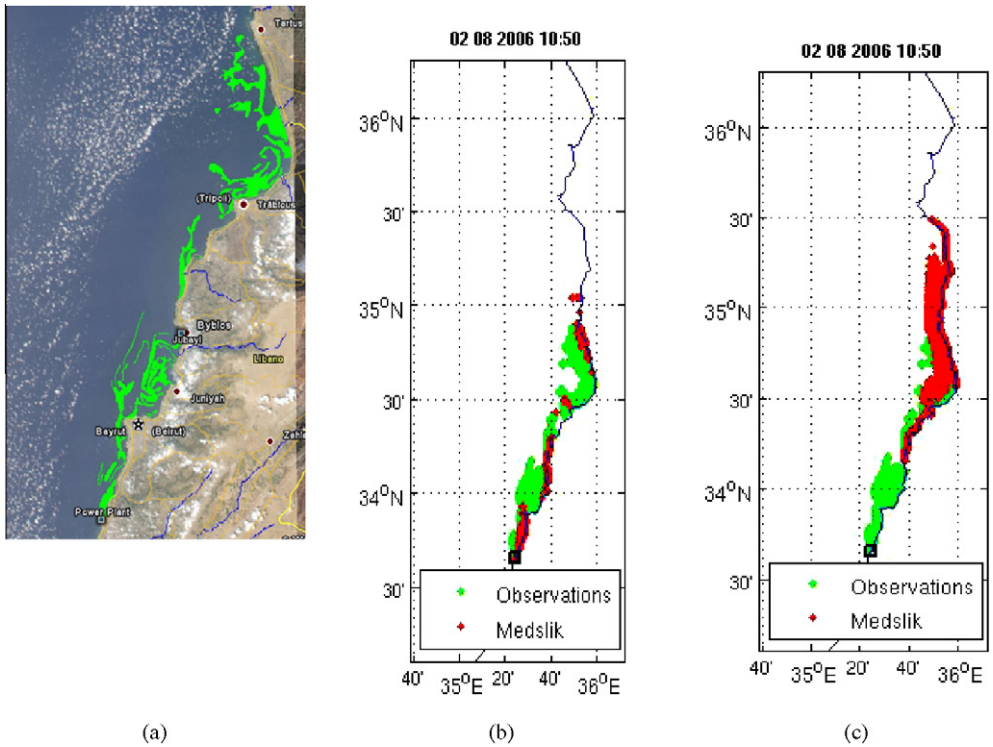

Fig. 10. Panel (a) shows the MODIS AQUA images from 2 August 2006 at 10:50 GMT. The observed positions of the oil slicks (panel a) are compared with the positions predicted by CYCOFOS (panel b) and by MFS (panel c). (a) Magnified portion of the MODIS AQUA image from 2 August at 10:50 GMT: Oil (green) is still located in the gulf between Tripoli and Tartus. There is no evidence of oil in the gulf between Tartus and Latakia. (b) The positions of the oil slicks and oil concentrations predicted by CYCOFOS for 2 August at 11:00 GMT (after 483 h) compared with the slick observed by MODIS (green), also shown in image 10 (a). (c) The positions of the oil slicks and oil concentrations predicted by MFS for 2 August at 11:00 GMT (after 483 h) compared with the slick observed by MODIS (green), also shown in image 10 (a).

Border (N34°38′27.3″–E035°58′22.3″), Hamidiye (N34°42′36.4″–E035°56′38.2″) and Resort (N34°44′37.4″–E035°55′54.1″). The latter location was, according to the Syrian Authorities, the northernmost area where oil pollution could be visually detected. Among the three Syrian sites visited, this beach appears the least affected by oil residues (IMO/REMPEC, 2006).

The CYCOFOS simulation showed oil deposition on the coast (Fig. 12b) extending northward and southward of Jieh. North of Jieh, the simulated oil deposition along the coast extended to Beirut, in agreement with the observations. The MFS simulation (Fig. 12c) did not show oil on the coast south of Jbeil, in contrast to the observations (Fig. 12a) of oil along the coast south of Jbeil

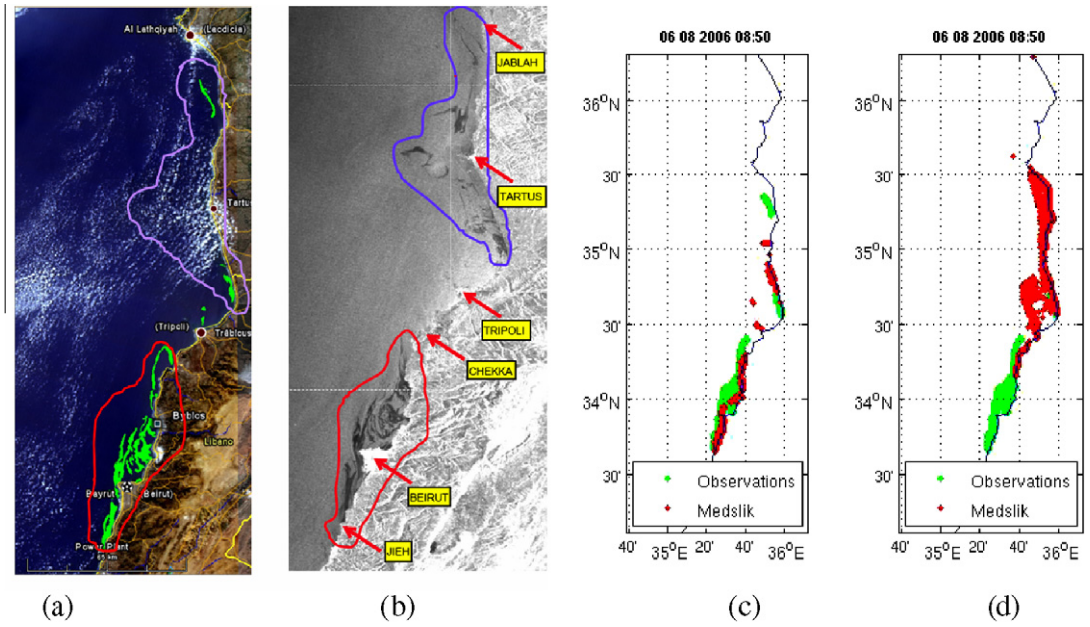

Fig. 11. Comparison of the following images for 6 August 2006: (a) MODIS TERRA image at 8:50 GMT; (b) ASAR image at 7:51 GMT, courtesy of ESA and JRC; (c) positions of the oil slicks predicted by CYCOFOS on 6 August at 9:00 GMT (after 576 h) and (d) positions of the oil slicks predicted by MFS on 6 August at 9:00 GMT (after 576 h).

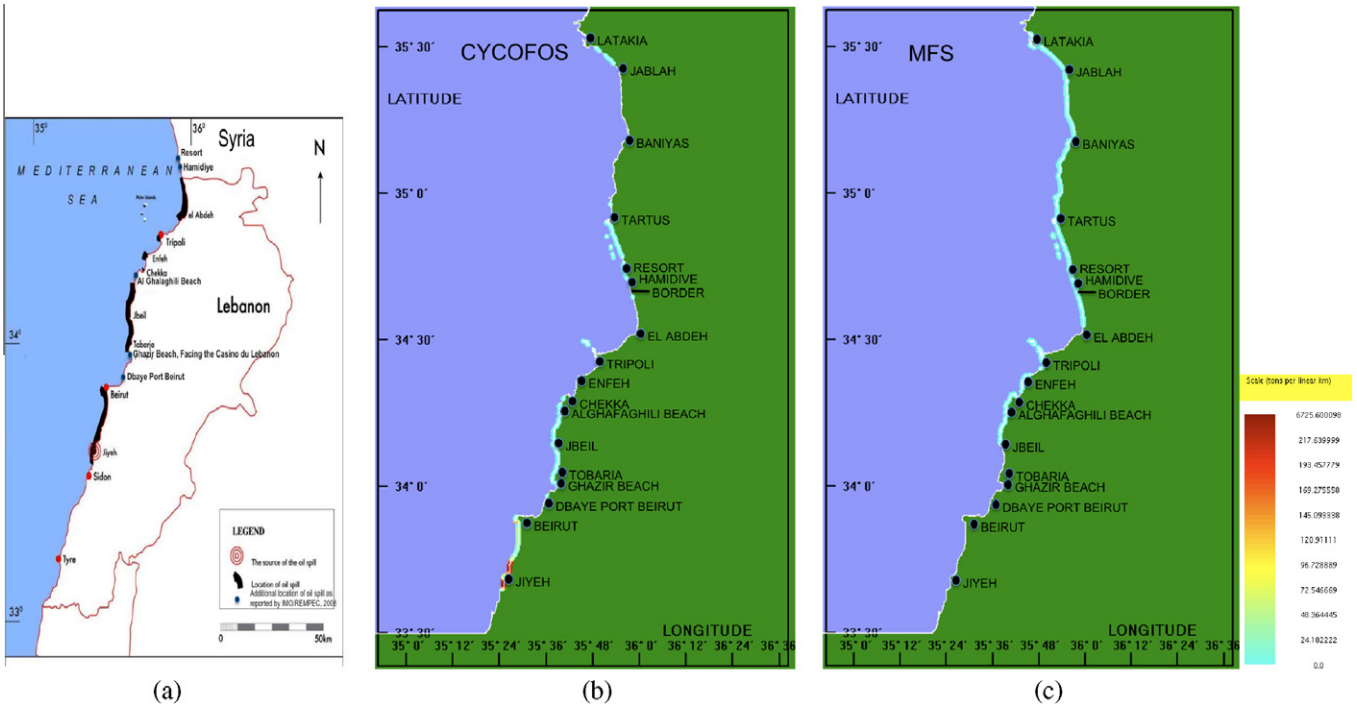

Fig. 12. Panel (a) shows the oil as observed along the Lebanese coastline by the Green Line association (GLA, 2007) integrated with the observations reported by the Experts Working Group for Lebanon in 2006 (EWGL, 2006). Panels (b) and (c) present the oil on the coast (tons per linear km) on 6 August 2006 as simulated by CYCOFOS (experiment 1) and MFS (experiment 6), respectively. The color palette is the same for panels (b) and (c).

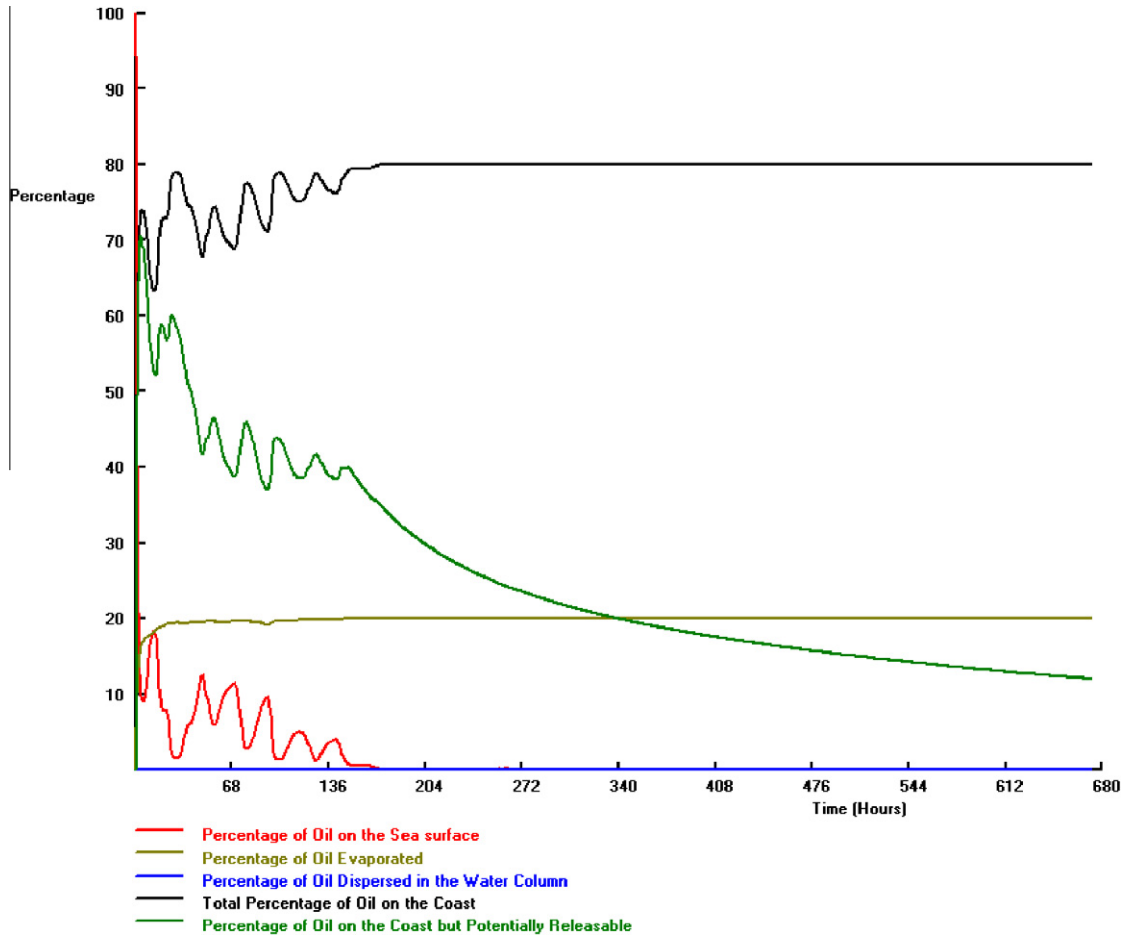

Fig. 13. Oil-fate parameters simulated by CYCOFOS (experiment 1) from 13 July 2006 to 6 August 2006.

(from Jiyeh to Beirut and from Ghazir to Jbeil). Oil was observed along the coast from Ghazir Beach to a position south of Chekka; these observations were closely reproduced by CYCOFOS and MFS (for only the area north of Jbeil). Between Chekka and Tripoli, oil was observed only at Enfeh and south of Tripoli. MFS simulation overestimated these observations, whereas CYCOFOS seemed to underestimate them. The oil observed along the coast between El Abdeh and the Lebanese/Syrian border was reproduced by MFS, which seemed to overestimate the oil north of Resort along the Syrian coast. The CYCOFOS simulation results (Fig. 12b) underestimated the oil observed between Abdeh and the Border while reproducing the observations in Hamidive and Resort but overestimated the oil north of Resort. CYCOFOS showed a small amount of oil south of Latakia, where the model forecast oil on the coast but no clear observation of oil was reported. MFS strongly overestimated the oil along this part of the Syrian coast.

The CYCOFOS simulation shows that the percentage of oil on the surface decreases as the percentage of oil on the coast increases (Fig. 13). The rate of absorption of oil onto the coast decreases as the existing coastal loading becomes larger; this implies that greater amounts of oil are available to re-enter the sea when the winds and currents are offshore. Within fewer than two days of the start of the incident, due to the high SST (Fig. 4), evaporation was high, and a little less than 20% of the original oil had evaporated (Fig. 13). The oil-fate graphs shows that after 28 days (672 h), 80% of the oil was on the coast as before, but about 10% of that remained free to move back to the sea. The model predicted that after eight days (192 h), less than 1% of the original oil was dispersed into the water column and less than 1% remained on the surface.

4.2. Sensitivity experiments

The sensitivity experiments were designed to test the impact of using water currents from MFS and CYCOFOS on the wind-factor and angle parameters and thus on the depth of the currents considered. The results of the sensitivity experiments are summarized in Fig. 14 for 23 July 2006. The simulations from CYCOFOS are presented in panels a, b and c, whereas those of MFS are shown in panels d, e and f.

Experiment 1 clearly reproduced the northward and coastal extent of the oil slick well, but it underestimated the offshore extent of the spill. Experiments 3 (Fig. 14b) and 5 (Fig. 14c), which incorporated surface currents and Stokes-drift parameterization, underestimated the northward extent of the oil slick. This pattern clearly shows that the CYCOFOS system fails to properly model the Ekman transport, probably due to sigma-layers displacement.

Fig. 14 also shows the MFS simulation results, which appear to be less sensitive overall to the model parameterization tested here. MFS experiment number 6 (Fig. 14f) seems to be the most appropriate. We conclude that MFS lacks the correct current amplitude because of its coarse resolution but that it adequately resolves the Ekman flow.

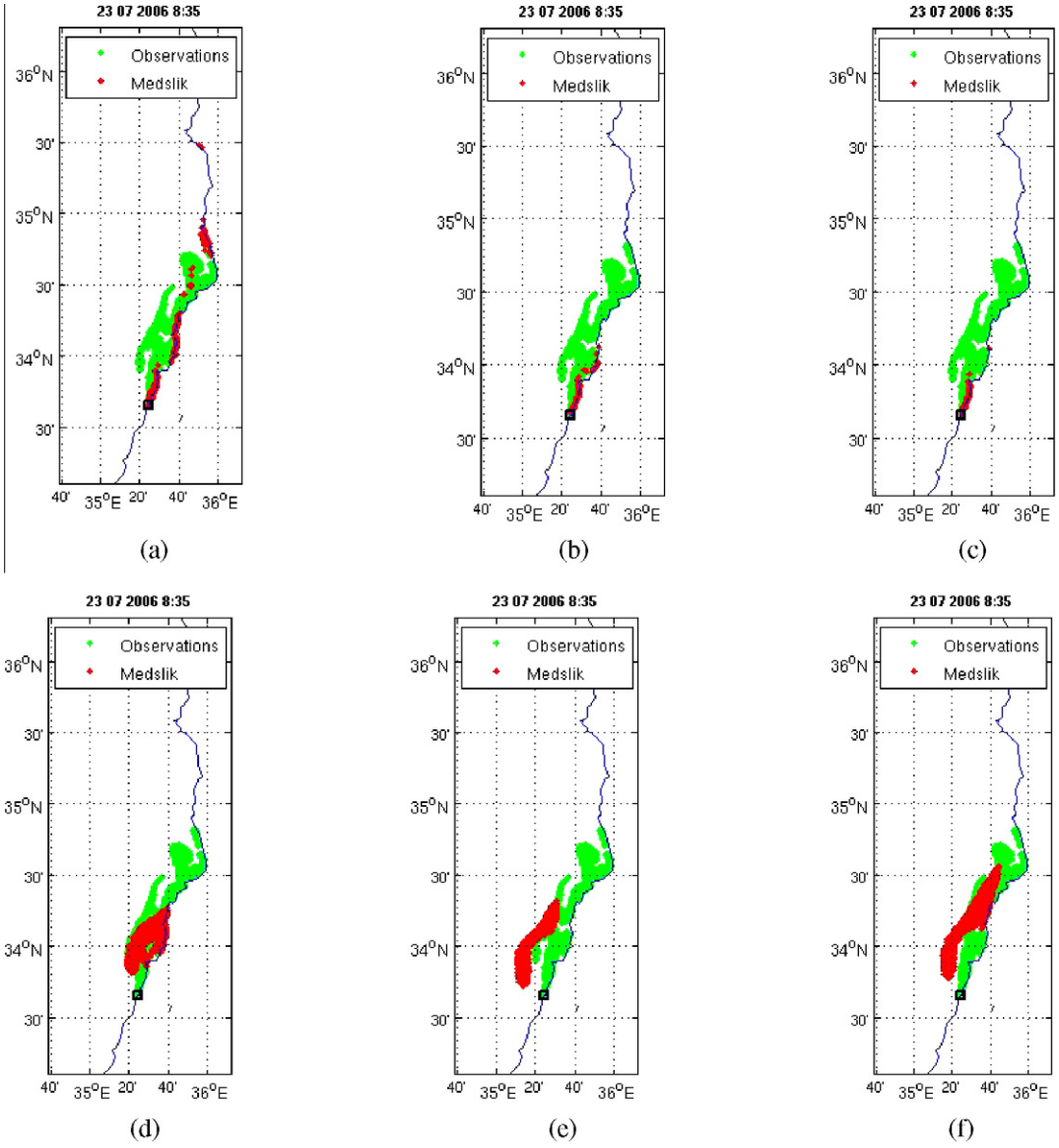

Fig. 14. Comparison of MFS and CYCOFOS simulations (red) for 23 July 2006 using different wind parameters and current depths and the oil-slick extent shown by the MODIS TERRA 8:35 GMT satellite image (green). (a) CYCOFOS; drift factor: 0.03; drift angle: 0°; Current depth = 30 m (experiment 1). (b) CYCOFOS; drift factor: 0; drift angle: 0°; Current depth = surface currents (experiment 3). (c) CYCOFOS; drift factor: 1.2%; drift angle: 0°; Current depth = surface (experiment 5). (d) MFS; drift factor: 0.03; drift angle: 0°; Current depth = 30 m (experiment 2). (e) MFS; drift factor: 0; drift angle: 0°; Current depth = surface currents (experiment 4). (f) MFS; drift factor: 1.2%; drift angle: 0°; Current depth = surface currents (experiment 6).

5. Conclusions

The Lebanon oil-pollution event is the largest such incident in the Eastern Mediterranean Sea to date. The oil spill affected most of the Lebanese coast and, as the oil spill drifted northward for more than a month, reached the southern Syrian coast. At the time of the Prestige oil-spill incident in 2002, only limited operational oceanographic products were available to assist the response agencies; certainly none were available at the time of the Haven oil-spill incident in 1991. During the entire period of the Lebanese oil-pollution crisis in July–August 2006, however, MOON was able to provide daily information on the displacement of the oil slicks.

This paper shows that the technological innovations provided by operational oceanography, which provides satellite images and real-time forecasts on currents, make it possible to precisely map oil-spill damage, even close to the coast. The satellite observing products used for oil-slick detection and for validation of the MEDSLIK oil-spill drift predictions are robust and capable of providing valuable operational information during this oil-spill accident.

Integration of different satellite sensors (ASAR, MODIS) during the Lebanon oil-spill event was a key element in monitoring the oil-spill incident appropriately and in a timely fashion. The integration of optical and SAR sensors on board satellites allows oil-drift evolution to be monitored in space and time at unprecedented resolution. Comparison of the MODIS and ASAR observations highlights (Fig. 11) that different satellite sensors can give similar results and that these can be used to validate the models.

Sensitivity experiments to different deterministic oil-spill drift factors show that the best results still require ad hoc tuning of parameters such as the current depth from the hydrodynamic model and the wind-drift factor and angle. These factors are considered to correct for the Ekman-drift velocities and Stokes drifts. Sensitivity experiments show that the best results for a relatively coarse MFS current field are obtained when the surface currents are corrected by a Stokes-drift factor (Rascle et al., 2006, 2008;

Ardhuin et al., 2009). For CYCOFOS, the deterministic part of the oil drift seems to be better parameterized with 30-m currents, a wind-drift factor of 3% and a wind-drift angle of 0°.

Our results indicate that both MFS and CYCOFOS models coupled to MEDSLIK are able to reproduce the timing and transport of the oil northward along the Lebanese and Syrian coasts. This comparison also shows that the CYCOFOS currents in MEDSLIK better represent the coastal trapping of the oil. This difference in performance is due to the higher horizontal resolution of the CYCOFOS forecasting system, which provides better resolution of the alongshore currents and allows the start of the oil spill to be placed closer to the coasts, near the real oil source.

MEDSLIK predicted that after six days, almost 80% of the original oil spilled at sea would be permanently landed along the Lebanese and South Syrian coasts, 20% of the original oil would be evaporated, and less than 1% of the oil would remain in the sea. The coastal impact was observed to be heaviest from Jieh up to south of Beirut, but significant impacts between Beirut and Chekka and northward along the Syrian coast were also reported. MEDSLIK coupled to MFS probably overestimated the northernmost part of the slick on the Syrian coast, even though the validation of this hindcast is difficult because the quantities of oil that reached the northern Syrian shores were not clearly reported.

The operational implementation of the MEDSLIK oil-spill model during the Lebanese oil-pollution crisis, using the CYCOFOS and SKIRON products, made it possible to provide the 'situation on the ground' to EU and UN agencies and other decision makers in the region and assisted them in drawing up an international action plan for the clean-up operations in response to the largest case of oil-spill pollution in the Eastern Mediterranean to date.

Acknowledgements

The paper was produced using the INGV MFS forecasting-system product and the OC-UCY CYCOFOS forecasting-system products. The MODIS satellite data products were processed at the GOS-CNR-ISAC Rome laboratory using the SeaDAS software developed by NASA GSFC, Greenbelt, Maryland, the HDFLook software developed by The Laboratoire d'Optique Atmosphérique, University of Lille, France, and the MS2GT tool box developed by the University of Colorado. Procedures for oil-spill detection were developed in the ENVI environment. Processed ENVISAT-ASAR data were made available by Telespazio and JRC. Part of this work was carried out with the support of the PRIMI project (ASI Contract No. I/094/06/0) financed by the Italian Space Agency (ASI).

References

Adamo, M., De Carolis, G., De Pasquale, V., Pasquariello, G., 2007. Exploiting sunglint signatures from meris and modis imagery in combination to SAR data to detect oil slicks. In: Proc. Envisat Symposium, ESA-SP-636.

Ahlstrom, S., 1975. A Mathematical Model for Predicting the Transport of Oil Slicks in Marine Waters. Res. Rept., Batelle Laboratories, Richland, WA.

Al-Rabeh, A.H., 1994. Estimating surface oil spill transport due to wind in the Arabian Gulf. Ocean Eng. 21 (5), 461–465.

Amato, E., Alcaro, L., 2006. Oil spill in Lebanon: in situ observations. In: Proceeding of the Workshop on Monitoring Activities Related to the Oil Pollution in Lebanon. European Commission Joint Research Centre, EUR 22531 EN.

Ardhuin, F., Marie, L., Rascle, N., Forget, P., Roland, A., 2009. Observation and estimation of lagrangian, stokes, and Eulerian currents induced by wind and waves at the sea surface. J. Phys. Oceanogr. 39 (11), 2820–2838.

Brenner, S., 2003. High-resolution nested model simulations of the climatological circulation in the southeastern corner of the Mediterranean Sea. Annal. Geophys. 21, 267–280.

Dobricic, S., Pinardi, N., 2008. An oceanographic three-dimensional assimilation scheme. Ocean Modell. 22, 89–105.

ECMWF, 2005. User Guide to ECMWF forecasts products Version 4.0, 14 March 2007. Meteorological Bulletin M3.2. Available from: <http://www.ecmwf.int/products/forecasts/guide/user_guide.pdf>.

EWGL (Experts Working Group For Lebanon), 2006. Lebanon marine and coastal oil pollution international assistance action plan.

Fingas, M.F., Brown, C.E., 1997. Review on oil spill remote sensing. Spill Sci. Technol. Bull. 4 (4), 199–208.

Fiscella, B., Giancaspro, A., Nirchio, F., Pavese, P., Trivero, P., 2000. Oil spill detection using marine SAR images. Int. J. Remote Sens. 21 (18), 3561–3566.

GLA (Green Line Association), 2007. Lebanon oil spill, July 2006 – July 2007.

Hunter, J.R., 1987. The application of Lagrangian particle tracking technique to modelling of dispersant in the sea. In: Noye, J. (Ed.), Numerical Modelling: Application to Marine Systems. Elsevier Science Publisher B.V., North-Holland.

Hu, C., Müller-Karger, F.E., Taylor, C., Myhre, D., Murch, B., Odriozola, A.L., 2003. MODIS detects oil spills in Lake Maracaibo, Venezuela. EOS 84 (33), 313–319.

IMO/REMPEC and Joint UNEP/OCHA, 2006. IMO/REMPEC and Joint UNEP/OCHA Environment Unit Mission in Syria, Final Report: Sampling at the Border between Syria and Lebanon (Ph. Rene Nijenhuis).

Jha, M.N., Levy, J., Gao, Y., 2008. Advances in remote sensing for oil spill disaster management: state-of-the-art sensors technology for oil spill surveillance. Sensors 8, 236–255.

Lardner, R.W., Zodiatis, G., 1998. An operational oil spill model in the Levantine Basin (Eastern Mediterranean Sea). Int. Symp. Mar. Pollut. 10, 5–9.

Lardner, R., Zodiatis, G., Hayes, D., Pinardi, N., 2006. Application of the MEDSLIK Oil Spill Model to the Lebanese Spill of July 2006. European Group of Experts on Satellite Monitoring of Sea Based Oil Pollution. European Communities.

Lotliker, A.A., Mupparthy, R.S., Srinivasa Kumar, T., Nayak, S.R., 2008. Evaluation of hi-resolution MODIS-aqua data for oil spill monitoring. In: Frouin, R.J., Andrefouet, S., Kawamura, H., Lynch, M.J., Pan, D., Platt, T. (Eds.), Remote Sensing of Inland, Coastal, and Oceanic Waters, Proceedings of SPIE, The International Society for Optical Engineering, vol. 7150. ISBN: 9780819473929.

Loureiro, M.L., Loomis, J.B., Vázquez, M.X., 2009. Economic valuation of environmental damages due to the prestige oil spill in Spain. Environ. Resour. Econ. 44 (4), 537–553.

Mackay, D., Paterson, S., 1980. Calculation of the evaporation rate of volatile liquids. In: Proc. 1980 National Conf. on Control of Hazardous Material Spills, Louiville, Ky.

Mackay, D., Leinonen, P.J., 1977. Mathematical model of the behaviour of oil spills on water with natural and chemical dispersion. Tech. Review Report No. EPS-3-EC-77-19, Fisheries and Environment, Canada.

Otremba, Z., Piskozub, J., 2001. Modelling of the optical contrast of an oil film on a sea surface. Opt. Express 9, 411–416.

Otremba, Z., Piskozub, J., 2004. Modelling the bidirectional reflectance distribution function (BRDF) of seawater polluted by an oil film. Opt. Express 12 (12), 1671–1676.

Pavlakis, P., Tarchi, D., Sieber, A., Ferraro, G., Vincent, G., 2001. On the Monitoring of Illicit Vessel Discharges: A Reconnaissance Study in the Mediterranean Sea. Joint Research Centre and DG – Environment. European Commission.

Pinardi, N., Allen, I., Demirov, E., De Mey, P., Korres, G., Lascaratos, A., et al., 2003. The Mediterranean ocean forecasting system: first phase of implementation (1998–2001). Ann. Geophys. 21, 3–20c.

Pinardi, N., Arneri, E., Crise, A., Ravaioli, M., Zavatarelli, M., 2006. The physical, sedimentary and ecological structure and variability of shelf areas in the Mediterranean Sea. In: Robinson, A.R., Brink, K. (Eds.), The Sea, vol. 14. Harvard University Press, Cambridge, USA, pp. 1243–1330.

Pond, S., Pickard, G.L., 1983. Introductory Dynamical Oceanography, second ed. Elsevier Butterworth-Heinemann.

Rascle, N., Ardhuin, F., Terray, E.A., 2006. Drift and mixing under the ocean surface: A coherent one-dimensional description with application to unstratified conditions. J. Geophys. Res. 111, C03016. doi:10.1029/2005JC003004.

Rascle, N., Ardhuin, F., Queffeulou, P., Croize-Fillon, D., 2008. A global wave parameter database for geophysical applications. Part 1: Wave-current-turbulence interaction parameters for the open ocean based on traditional parameterizations. Ocean Modelling 25 (3–4), 154–171.

Reed, M., Turner, C., Odulo, A., 1994. The role of wind and emulsification in modelling oil spill and surface drifter trajectories. Spill Sci. Technol. Bull. 1 (2), 143–157.

REMPEC, 2006. REMPEC News. From SITREP 12 (Updated 25.08.2006) Spill in Lebanon. Available from: <http://www.rempec.org/newsmore.asp?id=182&lang=en>.

Shi, L., Zhang, X., Seielstad, G., Zhao, C., He, M.-X., 2007. Oil spill detection by MODIS images using fuzzy cluster and texture feature extraction. Ocean Europe, 1–5.

Sofianos, S., Skliris, N., Mantziafou, A., Lascaratos, A., Zodiatis, G., Lardner, R., et al., 2006. Nesting operational forecasting models in the Eastern Mediterranean: active and slave mode. Ocean Sci. Discuss. 3, 1225–1254.

Tonani, M., Pinardi, N., Fratianni, C., Dobricic, S., 2008. A high resolution free surface model on the Mediterranean Sea. Ocean Sci. 4, 1–14.

UNEP, 2007. Lebanon Post-conflict Environmental Assessment. ISBN: 978-92-807-2794-4. Available from: <http://postconflict.unep.ch/publications.php?prog=lebanon>.

World Bank, 2007. Republic of Lebanon Economic Assessment of Environmental Degradation due to July 2006 Hostilities. World Bank.

Zodiatis, G., Lardner, R., Lascaratos, A., Georgiou, G., Korres, G., Syrimis, M., 2003. High resolution nested model for the Cyprus, NE Levantine Basin, Eastern Mediterranean Sea: implementation and climatological runs. Ann. Geophys. 21, 221–236.

Zodiatis, G., Lardner, R., Hayes, D., Soloviev, D., Georgiou, G., 2007. The successful application of the Mediterranean oil spill model in assisting the decision makers

during the oil pollution crisis of Lebanon in summer 2006. Rapp. Comm. Int. Mer. Medit. 214, 38.

Zodiatis, G., Lardner, R., Hayes, D., Georgiou, G., Sofianos, S., Skliris, N., et al., 2008a. Operational ocean forecasting in the Eastern Mediterranean: implementation and evaluation. Ocean Sci. 4, 31–47.

Zodiatis, G., Lardner R., Hayes D., Georgiou G., Pinardi N., De Dominicis M., Panayidou X., 2008b, The Mediterranean oil spill and trajectory prediction model in assisting the EU response agencies, Congreso Nacional de Salvamento en la Mar, Cadiz, 2–4 October, libro de actas, pp. 535–547.

Zodiatis, G., Hayes D., Lardner R., Georgiou G., Kallos G., Sofianos S., Pinardi N., Panayidou X., 2008c. Coastal and sub-regional operational marine core and downstream services in the Mediterranean Levantine Basin and their success in assisting the EU response agencies, IEEE CNF US/EU-Baltic.